An Analytical Model for Solute Redistribution during Solidification of Planar, Columnar, or Equiaxed Morphology

L. NASTAC and D.M. STEFANESCU

Existing models for solute redistribution (microsegregation) during solidification were reviewed. There are no analytical models that take into account limited diffusion in both the liquid and the solid phases. A new analytical mathematical model for solute redistribution was developed. Diffusion in liquid and in solid was considered. This model does not require a prescribed movement of the interface. It can be used for one-dimensional (1-D) (plate), two-dimensional (cylinder), or three-dimensional (3-D) (sphere) calculations. Thus, it is possible to calculate microsegregation at the level of primary or secondary arm spacing for columnar dendrites or for equiaxed dendrites. The solution was compared with calculations based on existing models, as well as with some available experimental data for the segregation of base elements in as cast Al-4.9 wt pct Cu, INCONEL 718, 625, and plain carbon (0.13 wt pct C) steel.

I. BACKGROUND

ASSESSMENT of microsegregation occurring in solidifying alloys is important, since it influences mechanical properties. Also, a comprehensive theoretical treatment of dendritic growth requires an accurate evaluation of the solutal field (microsegregation) during solidification. Models for calculation of microsegregation differ by the problem that they tackle as well as by the approach. Most models are restricted to the case of planar (plate) solidification (Figure 1(a)), or columnar solidification (Figure 1(b)), with the volume element over which the calculation is performed being selected between the primary or the secondary dendrite arms. One-dimensional (1-D) Cartesian or cylindrical coordinates solutions have been proposed. When equiaxed solidification is considered (Figure 1(c)) a three-dimensional (3-D) problem (or at least 1-D spherical coordinates) must be considered.

The earliest description of solute redistribution during solidification by Scheil[1] involves several assumptions, such as negligible undercooling during solidification, complete solute diffusion in liquid, no diffusion in solid, no mass flow into or out of the volume element, constant physical properties, and fixed volume element (no dendrite arm coarsening). However, the diffusion of solute into the solid phase can affect microsegregation significantly, especially toward the end of solidification. For example, calculations by Brooks *et al.*[2] showed that little solid-state diffusion occurs during the solidification and cooling of primary austenite solidified welds of Fe-Ni-Cr ternary alloys, whereas structures that solidify as ferrite may become almost completely homogenized as a result of diffusion. Although Brody and Flemings[3] (BF) have proposed a model that assumed complete diffusion in liquid and incomplete back diffusion, they have not solved the "Fickian" diffusion equation. When significant solid-state diffusion occurs, mass balance is violated. Consequently, the application of their result is limited to slow diffusion. Clyne and Kurz[4] (CK) have used the BF model and added a spline fit to match predictions by the Scheil equation and the equilibrium equation for infinitesimal and infinite diffusion coefficients, respectively. This relation has no physical basis. All these models are 1-D Cartesian and describe "plate" dendrite solidification.

The BF and CK analyses were used to explain microsegregation in Al-Cu and Al-Si alloys at cooling rates of up to 200 K/s by Sarreal and Abbaschian.[5] For higher cooling rates, a new equation based on the BF model that includes the effects of dendrite tip undercooling and eutectic temperature depression was developed.

Ohnaka[6] proposed models for plate (Figure 1(a)) and "columnar" dendrites (Figure 1(b)). Complete mixing in the liquid and parabolic growth were assumed. On the basis of an assumed profile, an equation for solute redistribution in the solid that includes the CK equation was derived:

$$C_S^* = kC_0 [1 - (1 - \beta k) f_S]^{k-1/1-\beta k} \qquad [1]$$

with

$$\beta = 2\gamma/(1 + 2\gamma) \qquad \text{and} \qquad \gamma = 4nD_S t_f/\lambda_1^2$$

where C_S^* is the interface concentration, λ_1 is the primary dendrite arm spacing, $n = 1$ for plate and $n = 2$ for columnar, and t_f is the local solidification time. Prior knowledge of the final solidification time is required. Note that for $D_S = 0$, this equation reduces to the Scheil equation, and for $D_S \to \infty$, it becomes the equilibrium equation. However, the diffusion equation was not directly solved.

Ogilvy and Kirkwood[7] further developed the BF model to allow for dendrite arm coarsening in binary and multicomponent alloys. For binary systems, the basic equation was

L. NASTAC, Graduate Research Assistant, and D.M. STEFANESCU, University Research Professor and Director of the Solidification Laboratory, are with the Department of Metallurgical and Materials Engineering, The University of Alabama, Tuscaloosa, AL 35487.

Manuscript submitted October 19, 1992.

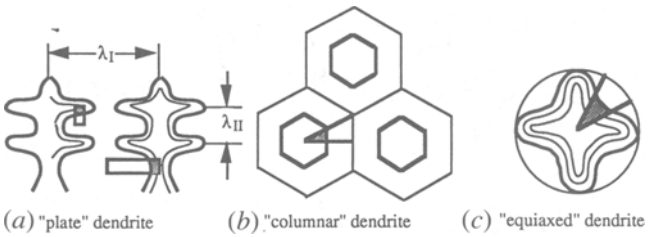

Fig. 1—Schematic representation of volume elements used in models for microsegregation.

$$C_L^*(1-k)\frac{dX}{dt} = D\frac{\partial C}{\partial x} + \frac{dC_L}{dt}\left(\frac{\lambda}{2} - X\right) + \frac{C_L - C_0}{2}\frac{d\lambda}{dt} \quad [2]$$

Here, X is the distance solidified. Thus, $f_s = 2X/\lambda$. The end term represents the increase in the size of the element due to arm coarsening, which brings in liquid of average composition that needs to be raised to the composition of the existing liquid. This equation was solved numerically under the additional assumptions of constant cooling rate and liquidus slope. Also, a correction factor for fast diffusing species was added.

Kobayashi[8] obtained exact analytical solutions for the plate and columnar dendrite models. Diffusion in solid was calculated, but complete liquid diffusion was again assumed. Solidification rate and physical properties, including partition coefficients, were considered constant. Linear solidification ($f_s = t/t_f$, where t_f is the final solidification time) was also assumed, which means that the motion of the interface was prescribed. The first-order approximate solution derived by Kobayashi reduces to Ohnaka's solution when applied to the interface. Calculations with the second-order approximate solution were very close to the exact solution. The equation is

$$C_S^* = kC_0\xi^{(k-1)/(1-\beta k)} \cdot \left\{1 + \Gamma\left[\frac{1}{2}(\xi^2 - 1) - 2(\xi^{-1} - 1) - \ln\xi\right]\right\} \quad [3]$$

with

$$\xi = 1 - (1 - \beta k)f_S \quad \text{and}$$

$$\Gamma = \beta^3 k(k-1)[(1+\beta)k - 2](4\gamma)^{-1}(1-\beta k)^{-3}$$

The model has been further extended to include a thermal model of solidification, multicomponent alloys, and temperature dependence of diffusivity. Note that again for $D_S = 0$, $\gamma = 0$, $\beta = 0$, $\Gamma = 0$, $\xi = 1 - f_s$, and this equation reduces to the Scheil equation. Also, for $D_S \to \infty$, it becomes the equilibrium equation. One of the major disadvantages of Kobayashi's solution is the large number of terms (20,000 for a Fourier number (Fo) = 0.05) required for convergence.[10]

Matsumiya *et al.*[9] developed a 1-D multicomponent numerical model in which both diffusions in liquid and solid were considered. Toward the end of solidification, especially for small partition ratios, lower liquid concentration than the analytical models was predicted.

Yeum *et al.*[10] proposed a finite difference method to describe microsegregation in a plate dendrite that allowed the use of variable k, D, and growth velocity. However, complete mixing in liquid was assumed.

Battle and Pehlke[11] developed a 1-D numerical model for plate dendrites that can be used either for the primary or for the secondary arm spacing. Diffusion was calculated in both liquid and solid, and dendrite arm coarsening was considered.

Further complications arise when multicomponent systems are considered. Chen and Chang[12] have proposed a numerical model for the geometrical description of the solid phases formed along the liquidus valley of a ternary system for plate dendrites. Constant growth velocity, variable partition ratios, and the BF model for diffusion were used.

This article introduces a complete analytical model for Fickian diffusion with temperature-independent diffusion coefficients and zero-flux boundary condition in systems solidifying with plate, columnar, or equiaxed morphology (Figure 1). The model takes into account solute transport in the solid and liquid phases and includes overall solute balance.

II. MODEL AND MATHEMATICAL FORMULATION

A. *Governing Equations and Boundary Conditions for Spherical Geometry*

Consider a spherical volume element within a liquid multicomponent alloy. A nucleus of radius R_n solidifies and eventually fills the whole volume element. The assumed geometry and the solute concentration profiles developed in the solid and liquid phases for one of the elements are presented schematically in Figure 2. Unconstrained, interface, or diffusion-controlled growth (equiaxed grain) may be considered. The microdiffusion

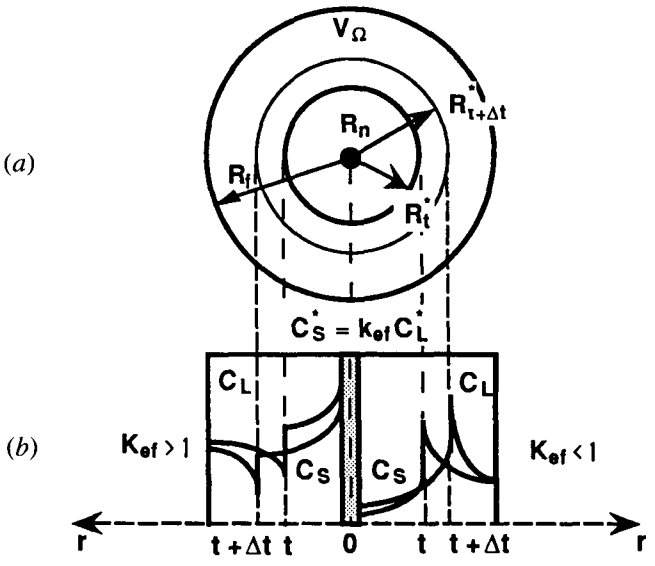

Fig. 2—Schematic representation of (*a*) a solidifying spherical element and (*b*) the associated concentration profile corresponding to a partition ratio greater or lower than one.

transport of the element starts concomitantly with solidification. The initial interface is at $r = R_n$, and it advances in the r direction until the solid/liquid interface radius, R^*, becomes equal to the radius of the volume element (grain), *i.e.*, $R^* = R_f$. Assuming that the volume element represents an equiaxed grain, the grain radius, R_f, can be calculated as

$$R_f = \left[\frac{4\pi}{3} N_g(x, y, z)\right]^{-1/3} \quad [4]$$

where N_g is the number of grains per unit volume (grain density), and x, y, and z are the coordinates of the microelement within the macrosystem. Since R_n is much smaller than the considered microelement, to simplify the analysis, it is taken as zero.

The problem to solve is to calculate the compositional profiles in both the solid and the liquid during solidification. Then, the microsegregation ratio can be calculated. At the nucleation temperature, $T_n \leq T_L$, the first solid formed has a solute concentration $k_{ef}C_0$. Here, k_{ef} is the partition ratio resulting from the combined influence of convection, interface kinetics, temperature, and composition (including third, fourth, *etc.* elements). The liquid in the vicinity of the solid/liquid interface is either enriched in (if $k_{ef} < 1$) or depleted of (if $k_{ef} > 1$) solute. The final liquid fraction achieves a solute concentration, C_{Lf}, which depends not only on the diffusion coefficients in the solid and liquid phases but also on the growth velocity of the grain. Two extreme cases can be considered. They both assume complete mixing in the liquid. The first one, *equilibrium solidification* (lever rule model), requires that diffusion in the solid and liquid phases be sufficiently fast to allow complete mixing necessary to maintain equilibrium. In this case, the final liquid fraction will have a concentration C_0/k_{ef}, where $k_{ef} = k$, which will solidify at T_s to give a solid of uniform concentration C_0. The second one, *nonequilibrium solidification*, assumes that diffusion in the liquid is rapid enough to allow complete mixing and no diffusion in the solid (Scheil model). Since there is no diffusion in the solid, the composition of the solid will finally reach the maximum solubility in the solid solution, or infinity (or zero), depending on the phase diagram. Although possible in principle such marginal behaviors are unlikely to occur in castings. Mostly, an intermediate behavior is expected.

The main assumptions of the model are as follows.

(1) Solute transport in both phases is by diffusion with diffusion coefficients independent of concentration; diffusion depends only on the r coordinate. Therefore, the double boundary problem must be solved for $C_S(r, t)$ and $C_L(r, t)$. The solute concentrations in the solid (s) and liquid (L) phases must each satisfy Fick's second law:

$$\frac{\partial C_S}{\partial t} = \frac{1}{r^m}\frac{\partial}{\partial r}\left(r^m D_S \frac{\partial C_S}{\partial r}\right) \quad \text{and}$$

$$\frac{\partial C_L}{\partial t} = \frac{1}{r^m}\frac{\partial}{\partial r}\left(r^m D_L \frac{\partial C_L}{\partial r}\right) \quad [5]$$

where D_S and D_L are the diffusion coefficients in the solid and liquid phases, respectively, and m is an exponent equal to two for spherical geometry. Equation [5] can also be used for plate or cylindrical geometry when m takes the value 0 or 1, respectively.

(2) The material is incompressible and the densities, ρ, in both phases are constant.

(3) The solid-liquid interface is planar and under local equilibrium. Then,

$$C_S^* = k_{ef}C_L^* \quad [6]$$

where the superscript[*] denotes values at the interface. From Eq. [6], two boundary conditions are obtained:

$$C_S[R^*(t), t] = C_S^* \quad \text{and} \quad C_L[R^*(t), t] = C_L^* \quad [7]$$

They are unknown *a priori*.

(4) There is no solute flow into or out of the volume element considered. Therefore, the overall mass balance can be written in integral form as

$$\frac{1}{\rho V_\Omega}\int_{V_\Omega} \rho C(r, t)\, dV_\Omega = C_0 \quad [8]$$

where C_0 is the initial concentration of the alloy and V_Ω is the volume of the element over which the mass balance is computed. Assuming that the densities of the solid and liquid phases are not only constant but also equal (this is only to simplify notations),

$$\int_{V_\Omega} C dV_\Omega = \int_0^{R^*} 4\pi r^2 C_S(r, t) dr + \int_{R^*}^{R_f} 4\pi r^2 C_L(r, t)\, dr \quad [9]$$

Equation [9] will be used to couple the concentration fields in both the solid and liquid phases.

The boundary conditions for the finite closed system are written as

$$D_S\frac{\partial C_S}{\partial r} = 0, \quad \text{at } r = 0 \quad \text{and}$$

$$D_L\frac{\partial C_L}{\partial r} = 0, \quad \text{at } r = R_f \quad [10]$$

(5) The initial concentration in the liquid, C_0, is a constant for each volume element (microscale) but can be a variable at the whole macroscale level (casting).

Finally, the solution of the coupled double boundary value problem can be obtained by solving Eq. [5] with the boundary conditions described by Eqs. [6], [7], and [10]. The liquid and solid solutal fields are coupled through Eq. [9]. The following initial conditions are used:

$$C_S(r, t_0) = k_{ef}C_0(x, y, z, t_0) \quad \text{and}$$

$$C_L(r, t_0) = C_0(x, y, z, t_0) \quad [11]$$

where t_0 is the time when the local solidifications starts. To simplify the notation, t_0 is taken as zero.

B. *Exact Solution of the Coupled Double Boundary Value Problem with Dimensional Quantities*

The exact solution of Eq. [5] for spherical geometry is described in detail in Appendix I for nondimensional quantities. Returning to the dimensional form, the solution of Fickian diffusion for a spherical element during solidification consists of the following equations:

$$C_S(r, t) = k_{ef}C_L^*(t) + k_{ef}[C_0 - C_L^*(t)] \sum_{n_S=1}^{\infty} \frac{B'_{nS}}{r} \sin[\sqrt{\lambda'_{n_S}} r] \exp[-\lambda'_{n_S} D_S t] \quad [12]$$

$$C_L(r, t) = C_L^*(t) + [C_0 - C_L^*(t)] \sum_{n_L=1}^{\infty} \frac{B'_{n_L}}{r} \sin[\sqrt{\lambda'_{n_L}}(r - R^*)] \cdot \exp[-\lambda'_{n_L} D_L t] \quad [13]$$

with

$$B_S = 2R^* \frac{(-1)^{n+1}}{n_S \pi} \qquad B'_{n_L} = \frac{2R^*}{\alpha_n} \quad [14]$$

$$\lambda'_{n_S} = \left[\frac{n_S \pi}{R^*}\right]^2 \quad \lambda'_{n_L} = \left[\frac{\alpha_n}{R_f - R^*}\right]^2 \quad \tan \alpha_n = \frac{R_f \alpha_n}{R_f - R^*} \quad [15]$$

The concentration at $r = 0$ can be calculated as

$$C_S(0, t) = k_{ef}C_L^*(t) + 2k_{ef}[C_0 - C_L^*(t)] \sum_{n_S=1}^{\infty} (-1)^{n_S+1} \cdot \exp[-\lambda'_{n_S} D_S t] \quad [16]$$

Similar derivations can be produced for plate and cylindrical geometry. The interface concentration is given by the general equation applicable to any geometry:

$$C_S^* = k_{ef}C_0 \left[1 - \frac{(1 - k_{ef})f_S}{1 - (m + 1)[k_{ef}I_S^{(m+1)} + I_L^{(m+1)}]}\right]^{-1} \quad [17]$$

where $f_S = (R^*/R_f)^{m+1}$ and I_S and I_L have different expressions as a function of geometry.

For spherical geometry,

$$I_S^{(3)} = \frac{2f_S}{\pi^2} \sum_{n=1}^{\infty} \frac{1}{n^2} \exp\left[-\left(\frac{n\pi}{f_S^{1/3}}\right)^2 \frac{D_S t}{R_f^2}\right]$$

and

$$I_L^{(3)} = 2f_S^{2/3}(1 - f_S^{1/3}) \sum_{n=1}^{\infty} \frac{1}{\alpha_n^2} \exp\left[-\left(\frac{\alpha_n}{1 - f_S^{1/3}}\right)^2 \frac{D_L t}{R_f^2}\right] \quad [18]$$

where α_n is the nth root of the equation $\alpha_n/\tan(\alpha_n) = 1 - f_S^{1/3}$.

For cylindrical geometry,

$$I_S^{(2)} = 2f_S \sum_{n=1}^{\infty} \frac{1}{z_{0_n}^2} \exp\left[-\frac{z_{0_n}^2}{f_S} \frac{D_S t}{R_f^2}\right]$$

and

$$I_L^{(2)} = 2(1 - f_S^{1/2})^2 \sum_{n=1}^{\infty} \frac{1}{z_{1_{n+1}}^2} \exp\left[-\left(\frac{z_{1_{n+1}}}{1 - f_S^{1/2}}\right)^2 \frac{D_L t}{R_f^2}\right] \quad [19]$$

where z_{0_n} and z_{1_n} are the nth root of Bessel functions of zero and first order, respectively.[25]

For plate geometry,

$$I_S^{(1)} = \frac{2f_S}{\pi^2} \sum_{n=1}^{\infty} \frac{1}{(n-0.5)^2} \exp\left[-\left(\frac{(n-0.5)\pi}{f_S}\right)^2 \frac{D_S t}{R_f^2}\right]$$

and

$$I_L^{(1)} = \frac{2}{\pi^2}(1 - f_S) \sum_{n=1}^{\infty} \frac{1}{(n-0.5)^2} \exp\left[-\left(\frac{(n-0.5)\pi}{1-f_S}\right)^2 \frac{D_L t}{R_f^2}\right] \quad [20]$$

This model allows a comprehensive treatment of dendritic or eutectic solidification. This is accomplished through calculation of the fraction of solid, or more precisely of R^*, with a heat transfer-transformation kinetics model.[13,14] For example, the growth velocity of the grain (interface) can be expressed as

$$V_g(t) = \frac{\partial R^*(t)}{\partial t} = \mu[\Delta T^*(t)]^2 \quad [21]$$

where ΔT^* is the interface undercooling and the growth constant, μ, can be either roughly estimated or determined from experiments.

C. *Quasi Steady-State Solution for Spherical Geometry*

Under the assumption of constant growth velocity, two dimensionless quantities can be further defined as

$$\xi = \frac{r}{R_f} - V_g \frac{t}{R_f} \quad \text{and} \quad t' = t \quad [22]$$

Then, for $m = 2$, Eqs. [5] become

$$\frac{1}{\xi^2}\frac{\partial}{\partial \xi}\left(\xi^2 \frac{\partial C_S}{\partial \xi}\right) + \frac{V_g R_f}{D_S}\frac{\partial C_S}{\partial \xi} = 0 \quad \text{and}$$

$$\frac{1}{\xi^2}\frac{\partial}{\partial \xi}\left(\xi^2 \frac{\partial C_L}{\partial \xi}\right) + \frac{V_g R_f}{D_L}\frac{\partial C_L}{\partial \xi} = 0 \quad [23]$$

This is a suggested transformation from stationary to moving coordinates[22] and is identified as the characteristic Fickian diffusion equation of the quasi-steady state. Using the same types of boundary and initial conditions as discussed previously, the quasi-steady-state solution for the spherical geometry consists of the following equations:

$$C_S(r, t) = k_{ef}C_0 + k_{ef}[C_L^*(t) - C_0] \cdot \frac{V_g t}{r} \frac{1 - \exp\left(-\frac{V_g}{D_S} r\right)}{1 - \exp\left(-\frac{V_g^2 t}{D_S}\right)} \quad [24]$$

$$C_L(r, t) = C_0 + [C_L^*(t) - C_0] \cdot \frac{V_g t}{r} \frac{\exp\left[\frac{V_g}{D_L} R_f \left(1 - \frac{r}{R_f}\right)\right] - 1 - \frac{V_g}{D_L} R_f}{\exp\left[\frac{V_g}{D_L} R_f \left(1 - \frac{V_g t}{R_f}\right)\right] - 1 - \frac{V_g}{D_L} R_f} \quad [25]$$

$$C_S^* = k_{ef}C_0 \left[1 + \frac{(1 - k_{ef})\left[\frac{V_g t}{R_f}\right]^3}{3\left(1 - k_{ef}(D_S/D_L)^2 + A_S' + A_S'' + A_L' + A_L''\right)}\right]^{-1} \quad [26]$$

where

$$A_S' = \frac{k_{ef}\left(\frac{V_g^2 t}{D_L}\right)^2}{2\left[1 - \exp\left(-\frac{V_g^2 t}{D_S}\right)\right]}$$

$$A_L' = \frac{V_g^2 t}{D_L\left\{1 - \left(1 + \frac{V_g}{D_L} R_f\right) \exp\left[\frac{V_g}{D_L} R_f \left(\frac{V_g t}{R_f} - 1\right)\right]\right\}}$$

$$A_S'' = \frac{k_{ef} D_S V_g^2 t}{D_L^2\left[\exp\left(\frac{V_g^2 t}{D_S}\right) - 1\right]}$$

$$A_L'' = \frac{\left(\frac{V_g R_f}{D_L}\right)^2 \left(1 + \frac{V_g R_f}{D_L}\right)\left[\left(\frac{V_g t}{R_f}\right)^2 - 1\right]}{2\left\{\exp\left[\frac{V_g R_f}{D_L}\left(1 - \frac{V_g t}{R_f}\right)\right] - \left(1 + \frac{V_g R_f}{D_L}\right)\right\}} \quad [27]$$

While Eqs. [12] through [20] can be applied for time-dependent growth velocity, Eqs. [24] through [27] can be used only for constant growth velocity (quasi-steady state), where the interface radius is $R^* = V_g t$.

III. DISCUSSION AND VALIDATION

The "overall" solute balance in integral form, Eq. [9], rather than the flux condition at the interface (time-derivative form)[6,8] has been used for three reasons: (1) it is more conservative than the interface mass balance, (2) the solution does not require a prescribed movement of the interface or a final solidification time as required, for instance, by Kobayachi's solutions, and (3) unlike term-by-term differentiation of Fourier series, term-by-term integration is *always* valid.[19]

Equations [12] through [20] represent the final solute redistribution in the solid phase for spherical, cylindrical, and plate geometry. Note that for D_S, $D_L = \infty$, the series I_S, $I_L = 0$ and Eq. [17] becomes the equation for equilibrium solidification; that is,

$$C_S^* = \frac{k_{ef}C_0}{1 - (1 - k_{ef})f_S} \quad [28]$$

The equilibrium equation was also directly derived from the overall mass balance equation in the integral form.[27] For $D_S = 0$ and $D_L = \infty$, the series I_S converges *extremely slowly* to $f_S/3$, $f_S/2$, and f_S and $I_L = 0$. Thus, Eq. [17] takes the form

$$C_S^* = k_{ef}C_0 \frac{1 - k_{ef}f_S}{1 - f_S} \quad [29]$$

This is the first approximation of the Scheil equation (see Appendix II for details). Nevertheless, at $f_S = 0$, it yields $C_S^* = kC_0$, and at $f_S = 1$, it predicts $C_S^* \to \infty$. Thus, the two extreme cases, equilibrium solidification (lever rule model) and complete nonequilibrium solidification (Scheil model), can both be obtained from Eqs. [12] through [20]. Physically, such extremes are never attained.

Equation [17] can be readily used for calculation of microsegregation, although it contains series expansions, since a few terms are enough to obtain accurate data. In dimensional form, the number of terms required for convergence (Eqs. [Iu] and [Iv] from Appendix I) can be estimated as follows:

$$n = \max\{n_S, n_L\} = \max\{[f_S^{1/3}(\mathrm{Fo}_{D_S})^{-1/2}], [(1 - f_S^{1/3})(\mathrm{Fo}_{D_L})^{-1/2}]\} \quad [30]$$

where Fo_D is the mass transfer Fourier number.

Equation [30] can be used to find the number of terms for each solid fraction. For $f_S = 1$, $n = n_{\max} = (\mathrm{Fo}_{D_S})^{-1/2}$, where $n_{\max}$ is the maximum number of terms required for convergence. For instance, when Fo_{D_S} takes values from 1 to 10^{-6}, $n_{\max}$ takes values from 1 to 10^3. Usually, $\mathrm{Fo}_{D_S} \geq 10^{-2}$ and, therefore, $n_{\max} \leq 10$. Indeed, as shown in Figure 3, the solution obtained for $n = 10$ gives minimal error (less than 0.1 pct) as compared to the exact solution. In Figure 3, when $f_s = 1$, the mass transfer Fourier number for the solid phase is $\mathrm{Fo}_{D_S} = 10^{-2}$. The exact solution was calculated such that the difference between current ($n + 1$ terms) and previous solutions (n terms) was $\varepsilon \leq 10^{-6}$.

Results of calculation with the analytical model for spherical elements are plotted in Figure 4 for various diffusion and partition ratios. For small D_S and small diffusion time, the solution approaches nonequilibrium (infinity for $k_{ef} > 1$ and zero for $k_{ef} > 1$). For large D_S, the solution for final liquid composition approaches equilibrium; that is, $C_l/C_o = 1$. It can be seen that this model is stable for both large and small diffusion times.

As pointed out by Battle and Pehlke,[11] calculated microsegregation is very sensitive to the value of the partition ratio used. Thus, for accurate prediction of microsegregation, it is necessary to have correct data for k_{ef}. Unfortunately, limited experimental data on partition ratios are available.[14] The proposed model can be used to calculate k_{ef} from experimental data. For systems where

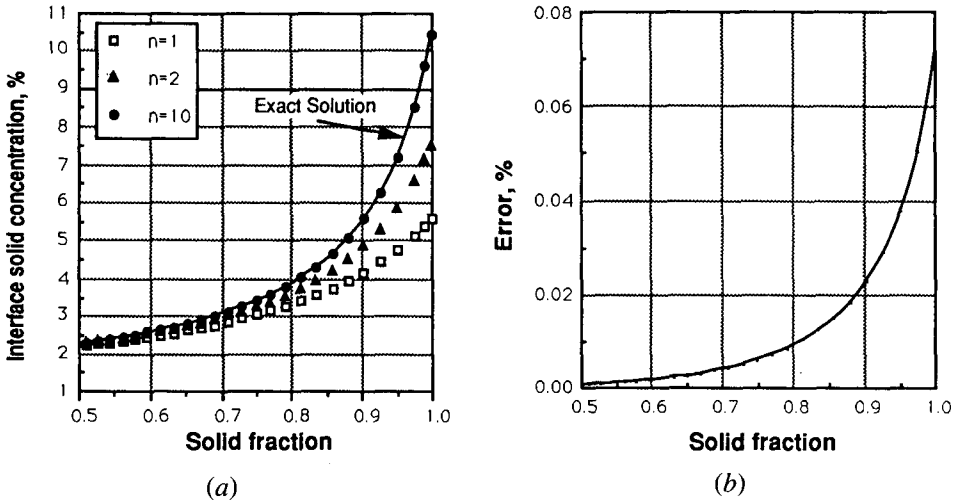

(a) (b)

Fig. 3—Comparison between calculated data with Eq. [17] for spherical geometry and different values of n, and (*a*) the exact solution and error for $n = 10$ as compared with (*b*) the exact solution.

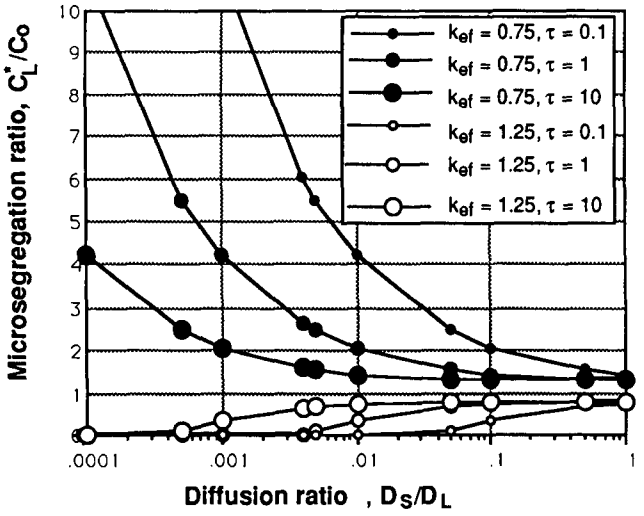

Fig. 4—Final microsegregation ratio (C_L/C_o) (spherical model) as a function of the diffusion ratio (D_S/D_L) for different partition ratios (k_{ef}) and three diffusional times ($\tau = D_L/R_f^2$).

microsegregation results in the solidification of an eutectic, k_{ef} can be calculated from Eq. [17], as follows:

$$k_{ef} = \frac{(C_0/C_E - 1)[1 - (m + 1)I_L^{(m+1)}] + 1 - f_E}{(C_0/C_E - 1)(m + 1)I_S^{(m+1)} + 1 - f_E} \quad [31]$$

where the fraction of eutectic is $f_E = 1 - f_S$ and C_E is the eutectic composition as given by the phase diagram. Then, if f_E is experimentally evaluated, Eq. [31] can be used to calculate the effective partition ratio for the particular solidification problem corresponding to the experiment. For systems where no second phase precipitates, k_{ef} can be calculated from Eq. [17] for $f_S = 1$ if the maximum interface composition at the end of solidification is known.

The effective partition ratio for an Al-4.9 wt pct Cu alloy was calculated with Eq. [31] using the diffusivities in Table I and the experimental data of Sarreal and Abbaschian[5] given in Table II. Plate geometry and constant growth velocity were assumed. The value of R_f was taken as half of the dendrite arm spacing. The results are given in Figure 5 for various cooling rates. As expected, k_{ef} is not affected significantly in the range of low cooling rates (0.1 to 1 K s^{-1}). On the contrary, for cooling rates above 1 K s^{-1}, k_{ef} increases rapidly.

A comparison of predictions of solute redistribution of niobium in INCONEL* 718 by various models is presented in Figure 6. These models include the Scheil, BF, CK, and Ohnaka models for plate elements, the Ohnaka model for columnar dendrite, and the newly proposed model for spherical and plate geometry. Also, the time-dependent and quasi-steady-state solutions of the proposed model are compared. The values of the physical parameters used in calculations are given in Table I. For this case, the quasi-steady-state solution seems to give poor results toward the end of solidification. However, it can be seen that for up to 0.9 fraction of solid, the quasi-steady-state solution almost coincides with the time-dependent one. Different models predict different composition profiles and final fractions of Laves phases. Since experimental data on the composition profile were not available for this case, validation can be done only against the final fraction of Laves phase. The proposed model for spherical geometry predicts 1.2 pct Laves, which is in the experimental range of 0.38 to 1.44 pct by volume Laves phase measured by Thompson *et al.*[23] All other models predict higher fractions. Thus, it appears that predictions by models assuming complete diffusion in liquid and plate elements applied to equiaxed geometry give correct results only accidentally.

To assess the validity of the new model not only in terms of final fraction of phase but also as to its accuracy in predicting the composition profile, calculated Nb redistribution for INCONEL 625 was plotted in Figure 7 against experimental data from directional solidified

*INCONEL is a trademark of Inco Alloys International, Inc., Huntington, WV.

Table I. Data Used in the Calculation of Concentration Profiles in Aluminum-Copper Superalloys and Steel

Figure	Element	D_S ($m^2\ s^{-1}$)	D_L ($m^2\ s^{-1}$)	R_f (μm)	k	t_f (s)	Reference
5	Cu	$18 \cdot 10^{-6} \exp(-125{,}520/RT)$	3×10^{-9}	Table II	0.145	Table II	5, 11
6	Nb	$56 \cdot 10^{-5} \exp(-2.8 \cdot 10^5/RT)$	1×10^{-9}	65	0.48	40	23
7	Nb	$56 \cdot 10^{-5} \exp(-2.8 \cdot 10^5/RT)$	1×10^{-9}	150	0.40	2060	24
8	Mn	$76 \cdot 10^{-6} \exp(-2.2 \cdot 10^5/RT)$	$38 \cdot 10^{-6} \exp(-69{,}000/RT)$	50	0.77	180	9
				180		960	
	P	$29 \cdot 10^{-5} \exp(-2.3 \cdot 10^5/RT)$	$13 \cdot 10^{-7} \exp(-99{,}000/RT)$	50	0.23	180	9
				180		960	

Table II. Data for Calculation of Partition Coefficients in Figure 5 for Al-4.9 Wt Pct Cu Alloys[5]

Cooling rate ($K\ s^{-1}$)	t_f (s)	R_f (μm)	Eutectic Fraction
0.1	980	45.5	0.0418
1.05	93.3	23	0.0490
11.25	8.72	11.5	0.0514
65	1.51	7	0.0537
187	0.52	5	0.0562
1700	0.058	2.7	0.0466

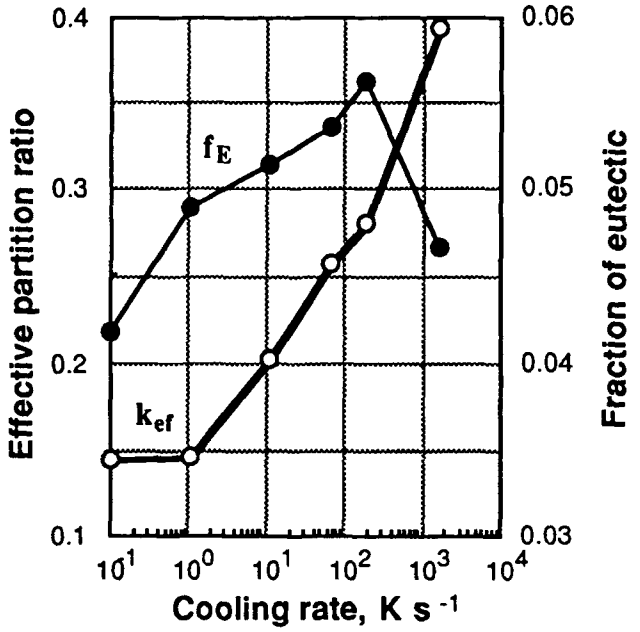

Fig. 5 — Influence of cooling rate on the calculated effective partition ratios and experimental[5] fraction of eutectic.

samples obtained by Sawai *et al.*[24] (Table I). Cylindrical geometry and constant growth velocity were assumed. Comparison was made with samples quenched from 1593 K, which is above the solidus temperature of 1523 K, and with samples quenched 2000 seconds after solidification, from 1423 K. Reasonably good agreement was obtained. It is considered that the agreement can be improved if an accurate transverse growth velocity is used. Note that existing analytical microsegregation models cannot be used for calculation after the end of solidification, since they rely on solidification time.

Additional validation was attempted for microsegregation of Mn and P in a plain carbon (0.13 wt pct C) steel directionally solidified with a columnar structure. Experimental data after Matsumiya *et al.*[9] were plotted in Figure 8 together with calculated data using the Scheil equation and the proposed model. Cylindrical geometry and constant growth velocity were assumed for the model. The data used in the calculation are given in Table I. Experimental data were available for two different cooling rates. At the slower cooling rate of 0.045 $K\ s^{-1}$, the dendrites in the microstructure did not exhibit clear patterns for secondary arms. Accordingly, calculations were performed for the primary arm spacing (R_f = 180 μm). When the cooling rate was increased to 0.25 $K\ s^{-1}$, the dendrites developed clear secondary arms. Thus, calculations with the model were performed for the secondary arm spacing (R_f = 50 μm) according to the experimental measurements. Unlike the Scheil model, the data obtained with the proposed model fit well the experimental results.

V. CONCLUDING REMARKS

A new analytical model that takes into account the solute transport not only in the solid phase (back diffusion) but also in the liquid phase was developed. The model was derived based on the Fickian diffusion in both phases, with zero-flux boundary conditions and overall solute balance. The overall solute balance in integral form rather then the flux condition at the interface (time-derivative form) has been used for three reasons. First, it is more conservative than the interface mass balance; second, the solution does not require a prescribed movement of the interface; and third, unlike term-by-term differentiation of Fourier series, term-by-term integration is always valid.

This model allows calculation of liquid and solid interface composition during and after solidification for volume elements with plate, cylindrical, or spherical geometry. Thus, it can be used to predict solute redistribution (microsegregation) for planar, columnar, or equiaxed morphology.

Prediction of solute redistribution depends on the accuracy of the partition ratio used in calculation. This ratio strongly depends on cooling rate, and very limited data are available in the literature. The proposed model can be used to calculate such data based on experimental values for the fraction of eutectic or for the maximum interface composition at the end of solidification.

Comparison of predictions through this model with

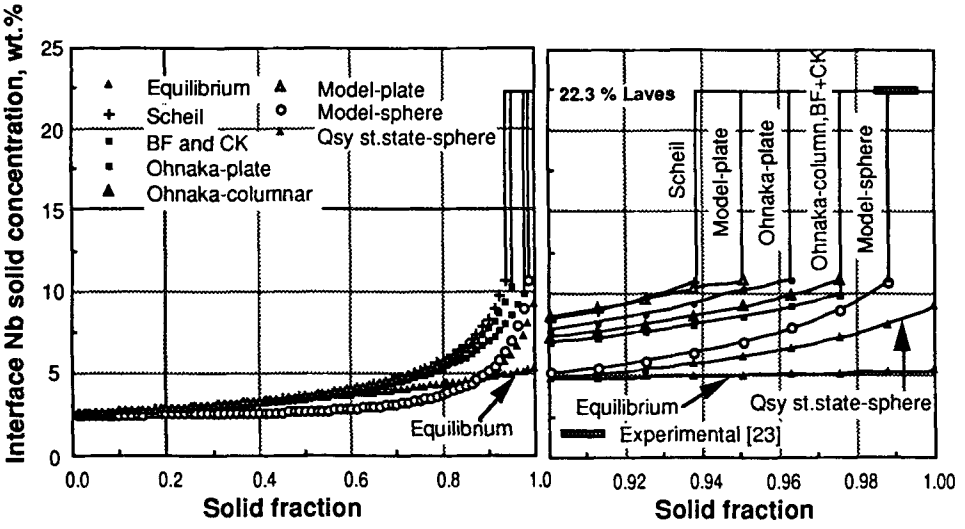

Fig. 6—Comparison of various models for Nb redistribution in INCONEL 718 solidified with equiaxed morphology. Initial Nb content was 5.25 wt pct.

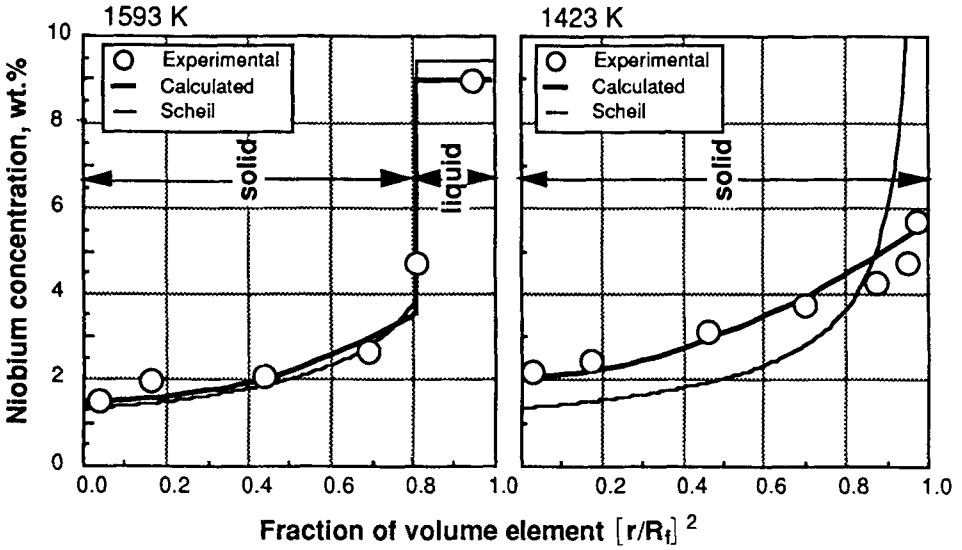

Fig. 7—Comparison of calculated (columnar and Scheil's model) and experimental data for Nb concentration across a columnar grain for samples quenched from 1593 K (f_S = 0.82) and from 1423 K (T_S = 1523 K). Initial Nb content was 3.21 wt pct.

experimental data for redistribution of copper in Al-4.9 wt pct Cu, niobium in INCONEL 625 and 718, and manganese and phosphorus in 0.13 wt pct C steel validated the correctness of the solution.

One of the important applications of this model is that it has been incorporated[26] into a model for the evolution of solid fraction of equiaxed dendrites used in heat transfer-transformation kinetics computer programs for casting.

APPENDIX I

Nondimensional analysis

The length scale is R_f. The time scale is

$$t = \frac{R_f^2}{D_L} \qquad [Ia]$$

On the basis of this time scale, the following dimensionless parameters can be defined:

$$V = V_g \frac{R_f}{D_L} \qquad D = \frac{D_S}{D_L} \qquad [Ib]$$

Also, the following dimensionless quantities are introduced:

$$a = \frac{r}{R_f} \qquad \tau = \frac{D_L t}{R_f^2} \qquad \eta = \frac{R^*}{R_f} = \int_0^\tau V(\tau) d\tau \qquad [Ic]$$

$$\theta_S = \frac{C_S - k_{ef} C_L^*}{k_{ef}(C_0 - C_L^*)} \qquad \theta_L = \frac{C_L - C_L^*}{C_0 - C_L^*} \qquad SR = \frac{C_L^*}{C_0} \qquad [Id]$$

where θ_S and θ_L are the dimensionless concentration in

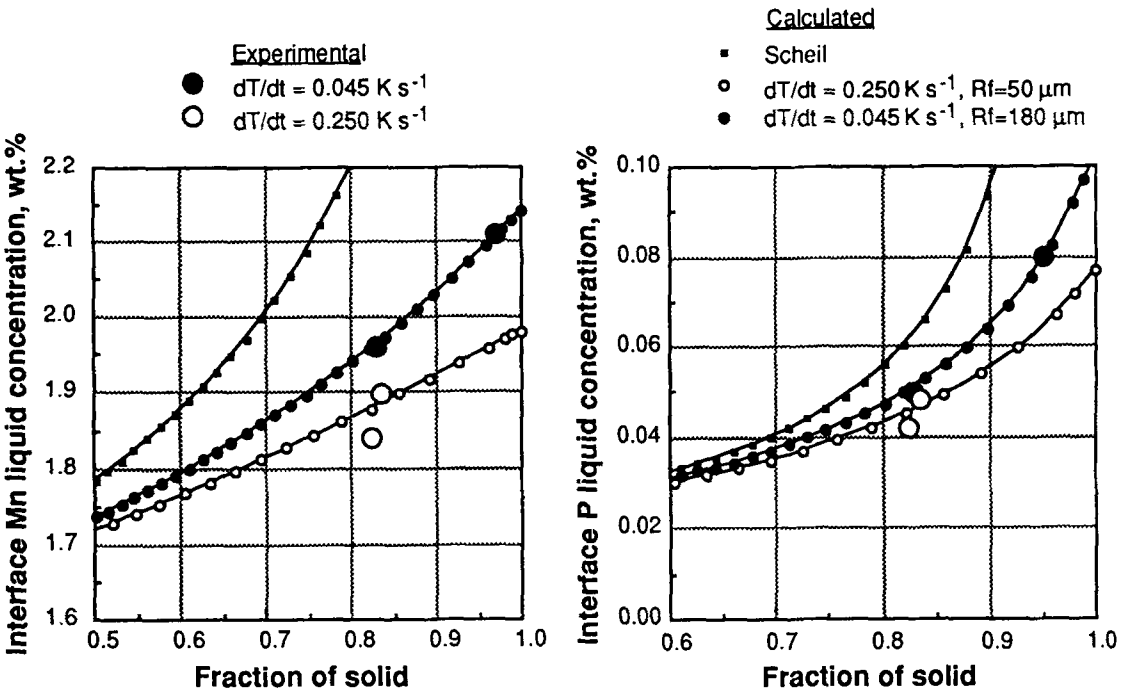

Fig. 8—Comparison of calculated (columnar and Scheil's model) and experimental liquid concentrations of Mn and P in steel solidified with columnar morphology. Initial Mn and P compositions were 1.52 and 0.016 pct, respectively.

the solid and the liquid, respectively, and SR is the instantaneous microsegregation ratio in the liquid.

The partial differential equations described in Eqs. [5] are linear and homogeneous with nonhomogeneous boundary conditions. They can be transformed into equations with homogeneous boundary condition.[19] Thus, we consider any *reference concentration distribution*, $u(r, t)$, with the property that it satisfies *only* the nonhomogeneous boundary conditions. For example, in the case of solid phase, this means that

$$\frac{\partial u(0, t)}{\partial r} = 0 \qquad \text{and} \qquad u[R^*(t), t] = C_S^*(t) \qquad \text{[Ie]}$$

Since the interface concentration, C_S^*, varies slowly with the diffusion time, which means that a quasi-steady state should be rapidly attained at the interface or that a local equilibrium exists at the interface, perhaps the best choice is the quasi-equilibrium solution; *i.e.*,

$$u(r, t) = B(t) + \frac{A(t)}{r} \qquad \text{[If]}$$

Applying the boundary conditions described in Eq. [Ie], the solution of Eq. [If] is

$$u(r, t) = C_S^*(t) \qquad \text{[Ig]}$$

The difference between the desired solution $c(r, t)$ and any chosen function $u(r, t)$ (*not necessarily* an equilibrium solution) is employed:

$$h(r, t) \equiv c(r, t) - u(r, t) \qquad \text{[Ih]}$$

Since both $c(r, t)$ and $u(r, t)$ satisfy the same linear but nonhomogeneous boundary conditions at both ends, it follows that $h(r, t)$ satisfies the *related* homogeneous boundary conditions, *e.g.*, Eq. [Ii].

The problem is then reduced to the solution of the following homogeneous boundary value problems:

$$\frac{\partial \theta_S}{\partial \tau} = D\frac{1}{a^2}\frac{\partial}{\partial a}\left(a^2\frac{\partial \theta_S}{\partial a}\right) \qquad \text{and}$$

$$\frac{\partial \theta_L}{\partial \tau} = \frac{1}{a^2}\frac{\partial}{\partial a}\left(a^2\frac{\partial \theta_L}{\partial a}\right) \qquad \text{[Ii]}$$

with the initial conditions

$$\theta_S(a, \tau_0) = 1, \qquad \text{for } C_S = k_{ef}C_0 \qquad \text{[Ij]}$$

$$\theta_L(a, \tau_0) = 1, \qquad \text{for } C_L = C_0 \qquad \text{[Ik]}$$

and the boundary conditions

$$D_S\frac{\partial \theta_S}{\partial a} = 0, \quad \text{for } a = 0 \qquad \frac{\partial \theta_L}{\partial a} = 0, \quad \text{for } a = 1$$

$$\theta[\eta(\tau), \tau] = 0 \qquad \theta_L[\eta(\tau), \tau] = 0 \qquad \text{[Il]}$$

The standard conservation law for solute in the dimensionless form is written as follows:

$$k_{ef}\int_0^{\eta(\tau)} a^2\theta_S(a, \tau)\, da + \int_{\eta(\tau)}^1 a^2\theta_L(a, \tau)\, da = \frac{SR[\eta(\tau)^3(1 - k_{ef}) - 1] + 1}{3(1 - SR)} \qquad \text{[Im]}$$

Denoting the first integral from Eq. [Im] as I_S and the second one as I_L, the microsegregation ratio is

$$SR = \frac{3(k_{ef}I_S + I_L) - 1}{3(k_{ef}I_S + I_L) + \eta(\tau)^3(1 - k_{ef}) - 1} \qquad \text{[In]}$$

To find I_S and I_L in Eq. [In], a solution of the coupled boundary value problem must be obtained.

Exact solution of the coupled double boundary value problem with nondimensional quantities

The solute transport during solidification of castings is a long time diffusion problem. In this case, the Fourier series rapidly converge.[15] Alternatively, the Laplace transform (*e.g.*, infinite summation of error functions) is well suited to short diffusion time problems (*e.g.*, laser treatment or welding, filament-matrix interaction in metal-matrix composites, and processing of amorphous alloys).

By using the substitution $F = \theta\, a$ into Eq. [Ii], the spherical diffusion problem is transformed into a planar one, with changing in boundary and initial conditions.[16,17]

Returning to the spherical system and assuming that the method of separation of variables still holds for this moving boundary problem, the general solutions in dimensionless form are as follows:

$$\theta_S = \left\{\frac{C_{S1}}{a}\cos[\sqrt{\lambda_S}a] + \frac{C_{S2}}{a}\sin[\sqrt{\lambda_S}a]\right\}\exp(-\lambda_S D_S \tau)$$

$$\theta_L = \left\{\frac{C_{L1}}{a}\cos[\sqrt{\lambda_L}(a-\eta)] + \frac{C_{L2}}{a}\sin[\sqrt{\lambda_L}(a-\eta)]\right\}\exp(-\lambda_L \tau) \qquad [Io]$$

where λ_S and λ_L are the eigenvalues and C_{S1}, C_{S2}, and C_{L1}, C_{L2} are constants for solid and liquid phases, respectively. The same type of solution can be found using Bessel functions in spherical coordinates.[18]

Applying the boundary conditions described by Eq. [II] and the principle of superposition extended,[19] the following product solutions are found:

$$\theta_S(a,\tau) = \sum_{nS=1}^{\infty}\frac{B_{n_S}}{a}\sin[\sqrt{\lambda_{n_S}}a]\exp[-\lambda_{n_S}D\tau]$$

$$\theta_L(a,\tau) = \sum_{nL=1}^{\infty}\frac{B_{n_L}}{a}\sin[\sqrt{\lambda_{n_L}}(a-\eta)]\exp[-\lambda_{n_L}\tau] \qquad [Ip]$$

with the eigenvalues

$$\lambda_S = \left[\frac{n\pi}{\eta}\right]^2 \quad \text{and} \quad \lambda_L = \left[\frac{\alpha_n}{1-\eta}\right]^2 \qquad [Iq]$$

where α_n is the nth root of the following transcendental equation:

$$\tan\alpha_n = \frac{\alpha_n}{1-\eta} \qquad [Ir]$$

Equation [Ir] can be solved by the perturbation,[20] series expansion, or numerical method. Since η varies in time from 0 to 1, this equation is difficult to solve, especially when η tends to 1, *i.e.*, α_n tends to the asymptotic formula, $(n - 1/2)\pi$. It was found that Muller's method,[21] unlike other numerical methods, converges always and very fast.

Next, applying the initial conditions, Eqs. [Ij] and [Ik] and the ortogonality of sines, one can solve for the coefficients B_{n_S} and B_{n_L}. Thus,

$$B_{n_S} = \frac{2}{\eta}\int_0^{\eta} a\sin[\sqrt{\lambda}a]\,da = 2\eta\frac{(-1)^{n+1}}{n\pi}$$

$$B_{n_L} = \frac{2}{1-\eta}\int_{\eta}^{1} a\sin[\sqrt{\lambda}(a-\eta)]\,da = \frac{2\eta}{\alpha_n} \qquad [Is]$$

A conservative estimate of the number (n_S or n_L) of terms required, such that the magnitude of the last series term retained is less than any desired number (Δ), is given by Unnam and Tenney[15] as a transcendental equation:

$$n = \frac{x}{\pi\sqrt{Dt}}\sqrt{\ln\frac{2}{n\pi\Delta}} \qquad [It]$$

where x is the characteristic length of the considered system.

A first approximation for this equation, which corresponds to $\Delta = 0.000033/n$, can be used to estimate the number of terms required for convergence:[15]

$$n = \frac{x}{\sqrt{Dt}} \qquad [Iu]$$

in nondimensional form, this equation can be written for both solutions as follows:

$$n_S \geq \frac{\eta}{\sqrt{D\tau}} \quad \text{and} \quad n_L \geq \frac{1-\eta}{\sqrt{\tau}} \qquad [Iv]$$

Finally, using the coupled Eq. [Im] and the final solutions in Eqs. [Ip], one can solve for the instantaneous microsegregation ratio, Eq. [In]. Thus,

$$I_S = \frac{2\eta^3}{\pi^2}\sum_{nS=1}^{\infty}\frac{1}{n_S^2}\exp\left[-\left(\frac{n_S\pi}{\eta}\right)^2 D\tau\right]$$

$$I_L = 2\eta^2(1-\eta)\sum_{n_L=1}^{\infty}\frac{1}{\alpha_{n_L}^2}\exp\left[-\left(\frac{\alpha_{n_L}}{1-\eta}\right)^2\tau\right] \qquad [Iw]$$

Since the growth velocity, V_g, is a function of time, to obtain the interface concentration profile, the analytical equations expressed by Eqs. [In], and [Iw] must be integrated in time.

Also, under the quasi-steady-state assumption, the growth velocity may be time independent. Consequently, the interface concentration profile may be directly predicted from the analytical solution without time integration.

APPENDIX II

It can be seen from the Fickian diffusion equations, Eqs. [5], that $D_S = 0$ is a singularity. This means that the Fickian model breaks down for $D_S = 0$. Also, for instance, Eq. [16] converges for $D_S > 0$ but does not converge for $D_S = 0$. Consequently, Eq. [29] should not be used for calculations. Note that Scheil's equation, while correct mathematically, was not derived on the

basis of the Fickian model but only on the basis of interface mass balance (first derivative of the overall mass balance). Accordingly, it should not be surprising that the model introduced in this article, which assumes Fickian diffusion and which was explicitly derived from the overall mass balance, cannot be simplified to the Scheil equation for $D_S = 0$.

However, it is interesting to note that Eq. [29] represents the first-order approximation of Scheil's equation. To prove it, let us consider Scheil's equation as

$$C_S^* = k_{ef} C_0 (1 - f_S)^{k_{ef}-1} = k_{ef} C_0 \frac{(1 - f_S)^{k_{ef}}}{1 - f_S} \quad [IIa]$$

This equation can be further expanded in Taylor's series, as follows:

$$C_S^* = k_{ef} C_0 \left[\frac{1}{(1 - f_S)} - \frac{k_{ef} f_S}{1!(1 - f_S)} + \frac{f_S^2 k_{ef}(k_{ef} - 1)}{2!(1 - f_S)} - \frac{f_S^3 (k_{ef} - 1)(k_{ef} - 2)}{3!(1 - f_S)} + \ldots \right] \quad [IIb]$$

The first two terms of this equation are identical with Eq. [29].

It is interesting to compare the general solution for very small solid diffusivity, Eq. [17], with the Scheil equation and with the first-order approximation, Eq. [29]. Results for calculation with assumed composition, partition ratio, and diffusivity are shown in Figure IIa. It can be seen that while, apparently, Scheil and Eq. [29] are very close over the whole solidification range, significant errors occur in the late stages of solidification. On the contrary, the general solution, Eq. [17], is extremely close to Scheil.

ACKNOWLEDGMENTS

This work was partially supported by Grant No. NAGW-1192 from NASA through Auburn University and by a grant from Caterpillar Inc. The authors would like to thank Dr. L. Hadji for his suggestions.

NOMENCLATURE

C	solute concentration (wt pct)
C_0	initial solute concentration (wt pct)
C_E	eutectic composition (wt pct)
D	diffusion coefficient (with subscript) ($m^2\ s^{-1}$) or diffusion ratio (without subscript)
Fo_{D_L}	mass transfer Fourier number for the liquid phase, $Fo_{D_L} = D_L t R_f^{-2}$
Fo_{D_S}	mass transfer Fourier number for the solid phase, $Fo_{D_S} = D_S t R_f^{-2}$
I	integrals defined in Appendix I
N_g	number of grains per unit volume (grain density) (m^{-3})
R_n	nucleus radius (m)
R	radius or characteristic length of the considered system (m)
SR	microsegregation ratio in the liquid
T_L	equilibrium liquidus temperature (K)
T_n	nucleation temperature (K)
T_S	solidus temperature (K)
V_Ω	volume of element (m^3)
V_g	growth velocity ($m\ s^{-1}$)
V	dimensionless velocity
X	position or characteristic length of the considered system (m)
a	dimensionless radius
f_E	eutectic fraction
f_S	solid fraction
h	function that satisfies the related homogeneous boundary conditions (Eq. [11])
k	equilibrium partition ratio
k_{ef}	effective partition ratio
m	index number in Eq. [5] that denotes the geometry
n	index number or number of series terms
r	radius coordinate (m)
t	time (s)

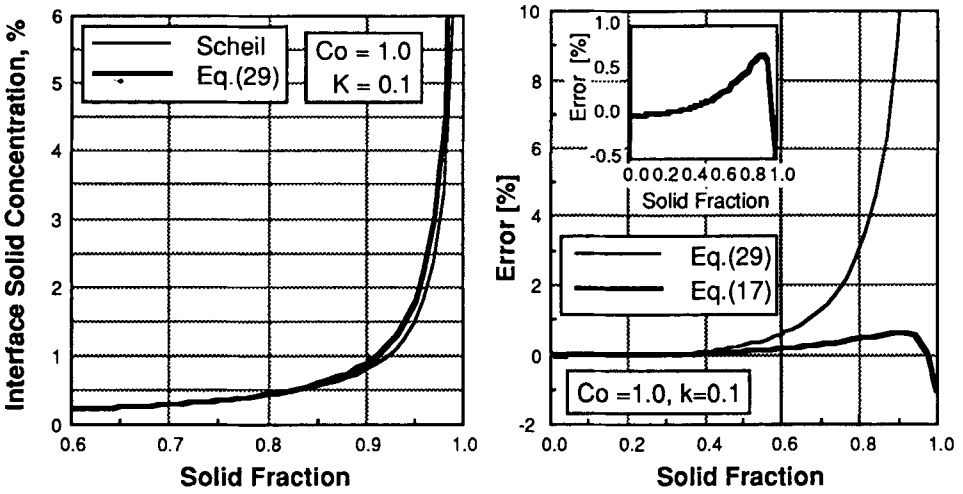

Fig. IIa—Comparison of calculated interface solid concentration (left) and of error for interface solid concentration (right). Eq. [17] was calculated with D_L, $Fo_{D_L} = \infty$, $D_S = 10^{-16}$, and $Fo_{D_S} = 10^{-6}$ ($f_S = 0$) to 10^{-4} ($f_S = 1$).

t_f	local solidification time (s)
u	any reference concentration distribution which satisfies only the nonhomogeneous boundary conditions
x, y, z	coordinates of the microelement within the macrosystem
z_{0_n}	nth root of Bessel functions of zero order
z_{1_n}	nth root of Bessel functions of first order
ΔT^*	interface undercooling (K)
Δt	time step (s)
α_n	nth root of Eq. [1r]
ρ	mass density of the alloy (kg m^{-3})
μ	growth constant (m s^{-1} K^{-2})
τ	dimensionless time
η	dimensionless interface position
θ	dimensionless concentration
λ	dendrite arm spacing (m)
λ_I	primary dendrite arm spacing (m)
λ_{II}	secondary dendrite arm spacing (m)
λ_n	eigenvalue (characteristic value)

General subscripts/superscripts

S	solid
L	liquid
f	final
$*$	at interface

REFERENCES

1. E. Scheil: *Zeitschrift Metallkde*, 1942, vol. 34, p. 70.
2. J.A. Brooks, M.I. Baskes, and F.A. Greulich: *Metall. Trans. A*, 1991, vol. 22A, pp. 915-26.
3. H.D. Brody and M.C. Flemings: *Trans. TMS-AIME*, 1966, vol. 236, p. 615.
4. T.W. Clyne and Kurz W.: *Metall. Trans. A*, 1981, vol. 12A, p. 965.
5. J.A. Sarreal and G.J. Abbaschian: *Metall. Trans. A*, 1986, vol. 17A, pp. 2063-73.
6. I. Ohnaka: *Trans. Iron Steel Inst. Jpn.*, 1986, vol. 26, pp. 1045-51.
7. A.J.W. Ogilvy and D.H. Kirkwood: *Appl. Scientific Res.*, 1987, vol. 44, pp. 43-49.
8. S. Kobayashi: *Trans. Iron Steel Inst. Jpn.*, 1988, vol. 28, pp. 728-35 and pp. 535-42.
9. T. Matsumiya, H. Kajioka, S. Mizoguchi, Y. Ueshima, and H. Esaka: *Trans. Iron Steel Inst. Jpn.*, 1984, vol. 24, pp. 873-82.
10. K.S. Yeum, V. Laxmanan, and D.R. Poirier: *Metall Trans. A*, 1989, vol. 20A, pp. 2847-56.
11. T.P. Battle and R.D. Pehlke: *Metall. Trans. B*, 1990, vol. 21B, pp. 357-75.
12. S.W. Chen and Y.A. Chang: *Metall Trans. A*, 1992, vol. 23A, pp. 1038-43.
13. D.M. Stefanescu, G. Upadhya, and D. Bandyopadhyay: *Metall. Trans. A*, 1990, vol. 21A, pp. 997-1005.
14. Thevoz Ph., J.L. Desbiolles, and M. Rappaz: *Metall. Trans. A*, 1989, vol. 20A, pp. 311-22.
15. J. Unnam and D.R. Tenney: *Metall. Trans. A*, 1981, vol. 12A, pp. 1369-72.
16. J. Crank: *The Mathematics of Diffusion*, Oxford University Press, London, 1964.
17. H.S. Carslaw and J.C. Jaeger: *Conduction of Heat in Solids*, Oxford University Press, London, 1959.
18. G.E. Myers: *Analytical Methods in Conduction Heat Transfer*, McGraw-Hill, New York, NY, 1971, pp. 126-29.
19. R. Haberman: *Elementary Applied Partial Differential Equations with Fourier Series and Boundary Value Problems*, 2nd ed., Prentice-Hall, Englewood Cliffs, NJ, 1987, pp. 246-61.
20. A. Aziz and T.Y. Na: *Perturbation Methods in Heat Transfer*, Series in Computational Methods in Mechanics and Thermal Sciences, Hemisphere Publishing Corp., New York, NY, 1984.
21. C.F. Gerald and P.O. Wheatley: *Applied Numerical Analysis*, 3rd ed., California Polytechnic State University, San Luis Obispo, 1986.
22. P.J. Schneider: *Conduction Heat Transfer*, Addison-Wesley Series in Mechanical Engineering, Addison-Wesley Publishing Co., Reading, MA, 1974, pp. 284-91.
23. R.G. Thompson, D.E. Mayo, and B. Radhakrishnan: *Metall. Trans. A*, 1991, vol. 22A, pp. 557-67.
24. T. Sawai, Y. Ueshima, and S. Mizoguchi: *Iron Steel Inst. Jpn. Int.*, 1990, vol. 30 (7), pp. 520-28.
25. M. Abramowitz and I.A. Stegun: *Handbook of Mathematical Functions*, Dover Publ., New York, NY, 1965, p. 409.
26. L. Nastac and D.M. Stefanescu: *Modeling of Casting, Welding, and Advanced Solidification Processes–VI*, TMS, 1993, pp. 209-17.
27. W. Kurz and D.J. Fisher: *Fundamentals of Solidification*, 3rd ed., Trans Tech Publications, Aedermannsdorf, Switzerland 1989.